

Article

Elemental Gains and Losses during Hydrothermal Alteration in Awak Mas Gold Deposit, Sulawesi Island, Indonesia: Constraints from Balanced Mineral Reactions

Ernowo Ernowo¹, Arifudin Idrus^{2,*}  and Franz Michael Meyer³¹ Geo-Resources Research Center, National Research and Innovation Agency, Jakarta 10340, Indonesia² Department of Geological Engineering, Universitas Gadjah Mada, Yogyakarta 55281, Indonesia³ Institute of Applied Mineralogy and Economic Geology, RWTH Aachen University, 52056 Aachen, Germany

* Correspondence: arifidrus@ugm.ac.id

Abstract: Hydrothermal gold mineralization is commonly associated with metasomatic processes resulting from interaction of hostrock with infiltrating hot aqueous fluids. Understanding of the alteration mechanism requires quantification of element changes in altered rock, relative to the unaltered or least-altered rock, representing the protolith. Balanced mineral reactions are used to gain quantitative insight into the alteration process associated with gold mineralization at the Awak Mas deposit. Three representative samples were carefully selected from the least-altered phyllite and the two alteration zones bordering the mineralization. Mineral mode, textural features, and mineral compositions were studied by microscopy and electron microprobe analyzer (EMPA). Quantitative modal analysis was performed with a Quanta 650 F QEMSCAN[®] system. The hydrothermal alteration sequence around the mineralization starts with the proximal albite–ankerite–pyrite alteration zone via the distal albite–chlorite alteration zone to the least-altered phyllite wall-rock. Balanced mineral reaction calculations were performed to evaluate elemental gains and losses. Most noticeable is the addition of Si, Na and Ca to each alteration zone. This alteration is represented by the almost complete replacement of muscovite by albite. The addition of Fe and S was highest in the albite–ankerite–pyrite alteration zone. Alteration of the least altered phyllite to the albite–chlorite zone involved a mass increase of 14.5% and a neglectable volume increase of 0.6%. The mass and a volume increase from the least altered phyllite to the albite–ankerite–pyrite zone was 40.5% and 0.47%, respectively. The very low volume change during alteration is also corroborated by the textural preservation indicating isovolumetric metasomatic reactions. The replacement of muscovite by albite may have had an important effect on the change of the rock failure mode from ductile to brittle, with consequences for the focusing of fluid flow.

Keywords: hydrothermal alteration; fluid flow; elemental gains and losses; orogenic gold; Awak Mas

Citation: Ernowo, E.; Idrus, A.; Meyer, F.M. Elemental Gains and Losses during Hydrothermal Alteration in Awak Mas Gold Deposit, Sulawesi Island, Indonesia: Constraints from Balanced Mineral Reactions. *Minerals* **2022**, *12*, 1630. <https://doi.org/10.3390/min12121630>

Academic Editors: Vasilios Melfos, Panagiotis Voudouris and Grigorios Aarne Sakellaris

Received: 10 November 2022

Accepted: 14 December 2022

Published: 17 December 2022

Publisher's Note: MDPI stays neutral with regard to jurisdictional claims in published maps and institutional affiliations.



Copyright: © 2022 by the authors. Licensee MDPI, Basel, Switzerland. This article is an open access article distributed under the terms and conditions of the Creative Commons Attribution (CC BY) license (<https://creativecommons.org/licenses/by/4.0/>).

1. Introduction

Fluids infiltrating and reacting with rocks during metamorphism and/or magmatism represent the most important open system process in the formation of orogenic gold deposits. Thus, orogenic Au deposits provide a valuable opportunity to investigate geochemical changes associated with structurally focused metasomatic activity [1–3].

Mass transfer calculations are quantitative tools used to monitor the fluid–rock interaction during the alteration and mineralization process. This provides information about the effects of overprinting metasomatism suffered by the altered rocks. Gresens [1] demonstrated that in order to calculate the mass change involved in fluid–rock reactions, the total mass per unit volume of the sample before and after the alteration must be known. One approach commonly used to solve this problem is to try to identify immobile elements [2–8].

An alternative approach was introduced by Dipple and Ferry [9], who calculated the time integrated molar fluid flux assuming chemical equilibrium between an aqueous

chloride fluid and the alteration assemblages. Quantification of mass transfer and fluid flux or fluid rock ratios are generally based on whole rock geochemistry, stable isotopes or the mineralogical composition [1,2,9–11]. The commonly observed large range in fluid–rock ratio estimates for the various methods may, however, be explained by differences in reaching equilibrium for a specific system under consideration [3,11]. In this study, we combine petrological observations, mineralogical quantification and mineral chemistry data in order to quantify mass transfer and volume change during alteration reactions in the Awak Mas gold deposit.

The Awak Mas gold deposit is in the Latimojong District, Luwu Regency, South Sulawesi Province, Republic of Indonesia. The location is about 350 km north of Makassar, the capital city of the South Sulawesi Province (Figure 1a). The Sulawesi Island is commonly divided into five tectonic provinces: (1) North Sulawesi Volcanic Province (arc-related igneous rocks), (2) Western Sulawesi Province (arc rocks and continental basement), (3) Central Sulawesi Metamorphic Belt, (4) East Sulawesi Ophiolite, and (5) other microcontinental fragments (East Arm and Buton) [12–16].

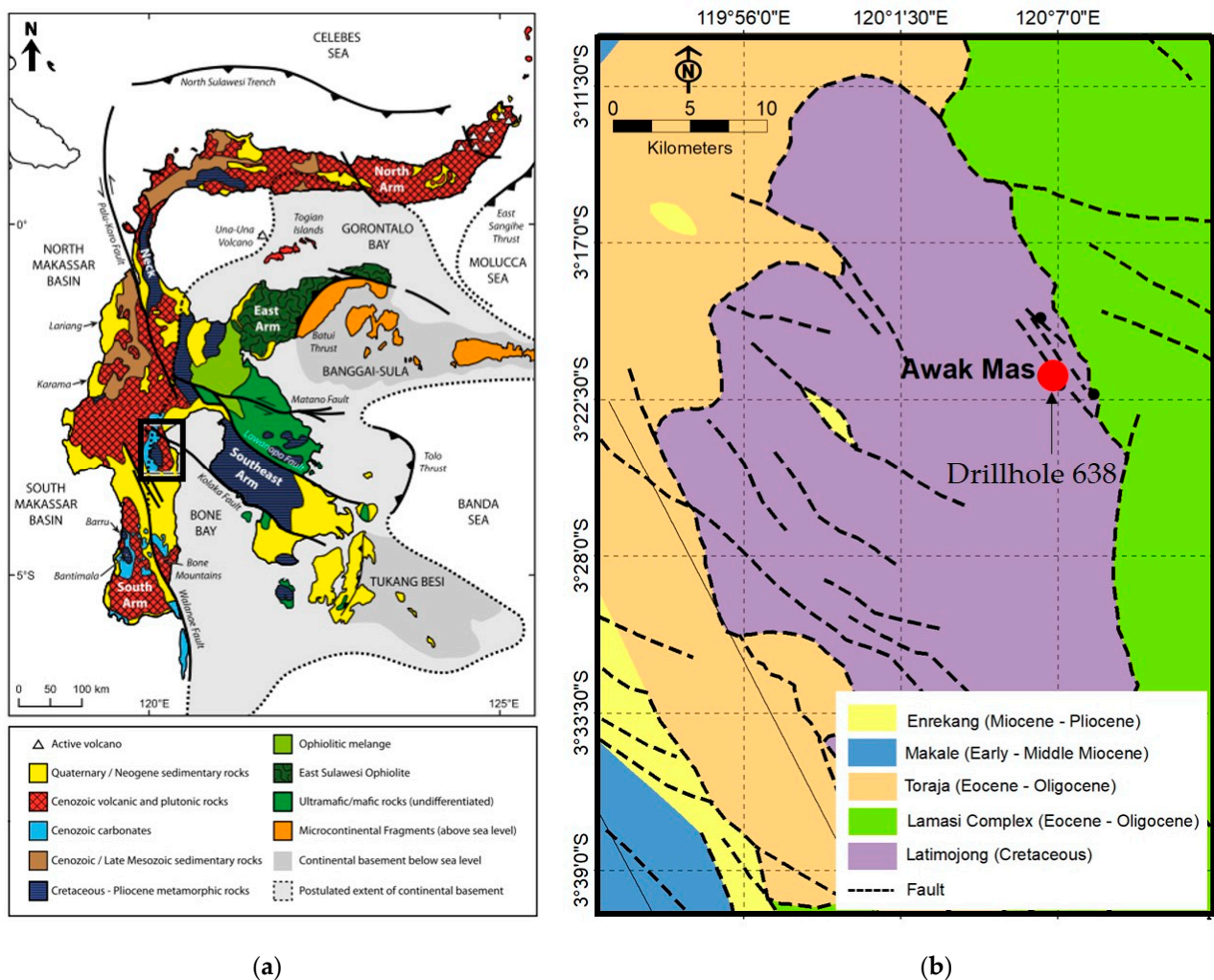


Figure 1. (a) Geology of Sulawesi Island, modified from [12], where the location of study area is shown by the black rectangle, (b) Geology of Awak Mas gold deposit, modified from [16–18]. The drillhole 638 location is shown by the red dot.

The Awak Mas gold deposit is situated in the southern arm of the Western Sulawesi Province, where both metamorphic basement units and arc-related igneous units prevail (Figure 1b). The Latimojong Formation is underlaid by phyllites, slates, basic to intermediate volcanics, limestones, and schists, representing a platform and/or fore arc trough flysch

sequence intruded by granite, diorite, monzonite, and/or syenite plugs and stocks [16–22]. The other lithological formation in this area is the Lamasi Complex, composed of mafic to intermediate rocks. The Toraja Group consists of lithologies originating from marine to shallow marine depositions, as well as carbonate rocks of the Makale Formation and the Enrekang volcanics [16–19].

Awak Mas is an orogenic gold deposit hosted by pumpellyite to greenschist facies metasedimentary and metavolcanic rocks [21,22]. The gold mineralization is spatially related to sulfide minerals within quartz–albite–ankerite and quartz–ankerite–siderite bordered quartz veins [22]. Pyrite is the most abundant sulfide, whereas galena and chalcopyrite are very minor. The mineralized quartz veins are encased by an alteration halo grading from the proximal albite–ankerite–pyrite alteration zone, via the distal albite–chlorite alteration zone into the least altered phyllite. The relation between alteration zones and the gold mineralization is sketched by the core log from drill hole number 638 (Figure 2). The highest gold content of up to 25 ppm occurs within the albite–ankerite–pyrite altered phyllite. The infiltrating aqueous ore fluid was found to be CO₂-poor and of low salinity at temperatures between 275 and 325 °C [22]. Fluid inclusion chemistry points to an origin of metamorphic dewatering of organic-rich marine sedimentary sequences [22].

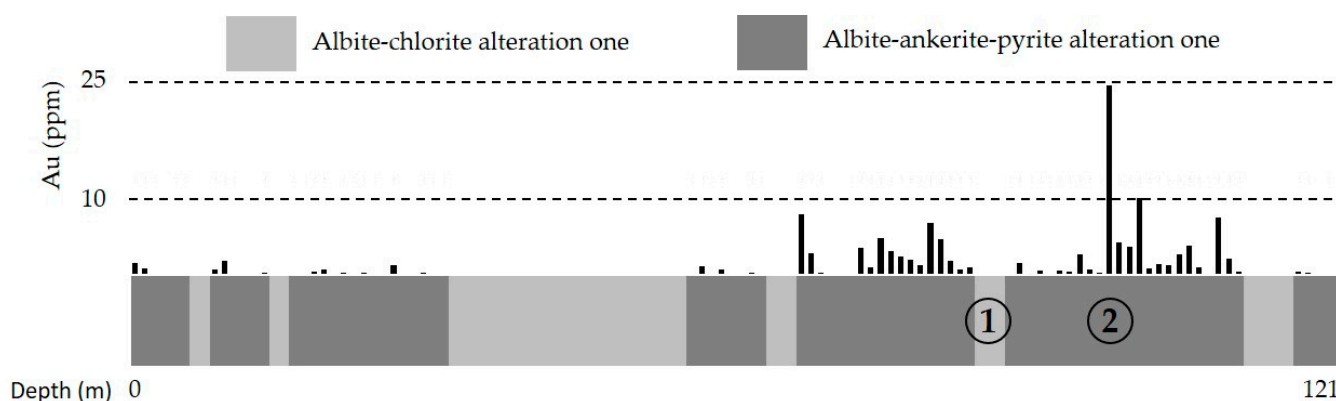


Figure 2. Sketch of core log of drill hole number 638 with the gold content [23]. 1 = sample of albite–chlorite alteration zone, 2 = sample of albite–ankerite–pyrite alteration zone.

2. Materials and Methods

Three representative bulk samples and polished sections were carefully selected from a fresh outcrop of host rock phyllites 5 m away from the collar of drill hole 638 and the two alteration zones exposed in the drill core (Figure 2). Microscopic studies were conducted to describe the petrography of the unaltered host-rocks and to identify the alteration assemblages. Bulk rock mineral assembly quantification was performed by a Quanta 650 F QEMSCAN[®] system at the Institute of Applied Mineralogy and Mineral Deposits, RWTH Aachen University. The instrument was equipped with a Bruker Dual X-Flash5030 energy dispersive X-ray (EDS) detector, operated with an accelerating voltage of 15 kV and a specimen current of approximately 10 nA. For spectral interpretation and data processing, the iDiscover v.5.2 software suite (FEI) was used. The analytical method used refers to the work of Gottlieb et al. [24], Pirrie et al. [25] and Sindern and Meyer [26].

The XRF analysis operated to determine the major element concentration in bulk samples was conducted at the IML Laboratory of Geochemistry and Environmental Analysis, RWTH Aachen University. Mineral compositions were analyzed to identify systematic chemical variations within the alteration zones. The analyses were carried out using a JEOL-JXA-8900R electron microprobe analyzer at the Institute of Applied Mineralogy and Mineral Deposits, RWTH Aachen University. Analyses of silicates and carbonates were performed at 15 kV between 19 and 24 nA. Sulfides and oxides were analyzed at 25 kV between 25 and 27 nA. The measurements were calibrated with natural sulfide, oxide and silicate mineral standards for specific elements.

3. Results

3.1. Mineralogy

The least altered phyllite exhibits well-established foliation and consists of fine-grained muscovite, albite, chlorite, quartz and biotite (Figure 3a). The albite is mostly altered to muscovite. The accessory minerals occupying a volume of less than 1% are rutile, kaolinite and pyrite.

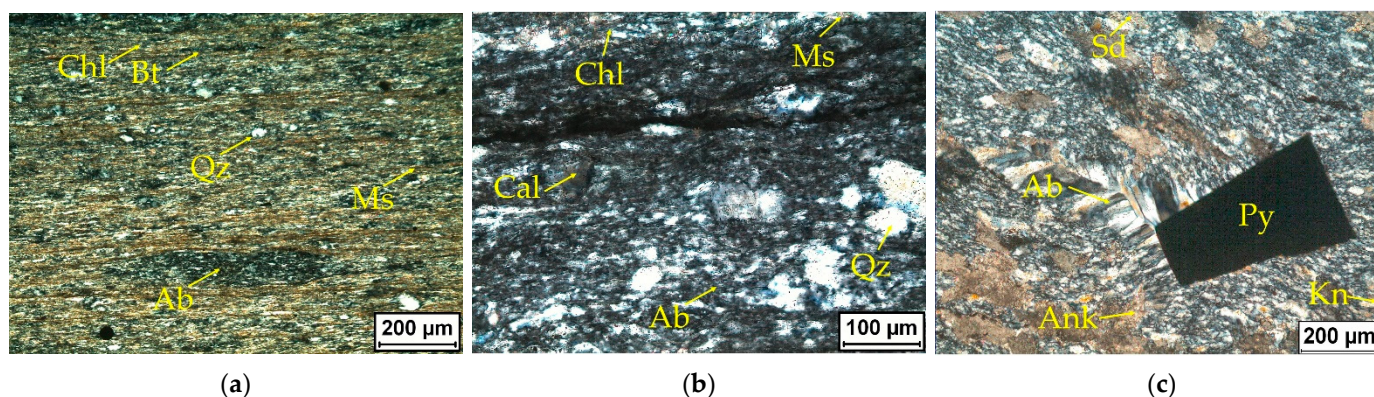


Figure 3. Photomicrograph of: (a) Least altered phyllite (b) Albite–chlorite alteration zone, and (c) Albite–ankerite–pyrite alteration zone. Abbreviations: Ab = albite, Ank = ankerite, Bt = biotite, Cal = calcite, Chl = chlorite, Kn = kaolinite, Ms = muscovite, Py = pyrite, Qz = quartz, Sd = siderite.

Samples from the albite–chlorite alteration zone are strongly foliated and cross-cut by thin quartz–calcite veins and veinlets. The mineralogical composition of the albite–chlorite alteration is predominantly albite followed by chlorite, calcite, muscovite and quartz. In addition, accessory minerals, such as rutile and pyrite, occupy a volume of less than 1%. The main secondary minerals that are formed by hydrothermal alteration in this zone are albite, chlorite and calcite, which are also present in the least altered phyllites to varying degrees. Chlorite and albite replace the matrix as well as detrital grains of muscovite along foliation (Figure 3b). Calcite occurs in fractures and replaces rock fragments as disseminated grains. Minor kaolinite is probably a supergene replacement of Fe-bearing minerals.

The albite–ankerite–pyrite alteration zone is composed of albite, ankerite, pyrite and siderite. The accessory minerals occupying a volume of less than 1% are muscovite, quartz, kaolinite and rutile. The dominant secondary mineral is albite, which almost totally replaces muscovite and chlorite by maintaining the foliation structure (Figure 2c). Disseminated pyrite replaces the Fe-bearing minerals (muscovite, chlorite and ankerite) along the sheared foliation, as well as porphyroblast.

The mineral distribution map and modal mineral analysis by QEMSCAN of the least altered phyllite and the two alteration zones is summarized in Figures 4 and 5 and Table 1. Chalcopyrite, smectite, apatite, zircon, Fe-rim and chromite amounts are less than 1% and are not detected by the EPMA measurements are therefore ignored in the calculations of this study. Dolomite chemical calculations fall into the ankerite category. In the least altered phyllite, muscovite is the predominant mineral component (56%), followed by albite (~18%), chlorite (~12%), quartz (~8%), biotite (~3%), rutile (~1%) and pyrite (~1%).

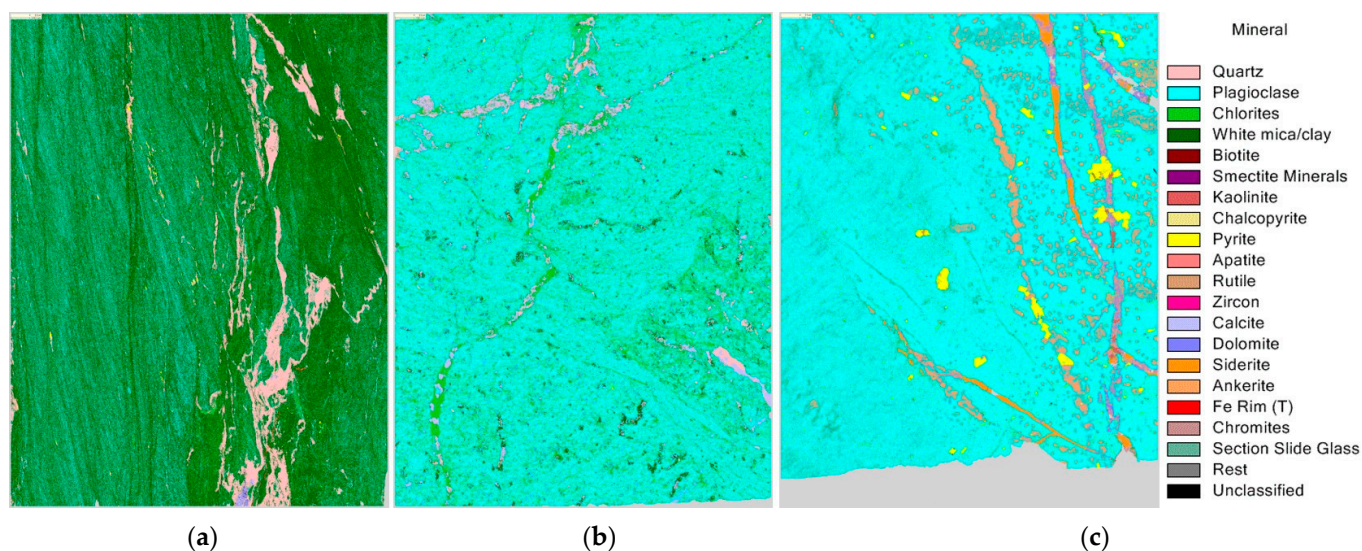


Figure 4. Mineral map by QEMSCAN analysis showing the distribution minerals in the (a) least altered phyllite, (b) albite–chlorite alteration zone, and (c) albite–ankerite–pyrite alteration zone. (Plagioclase = albite, white mica = muscovite).

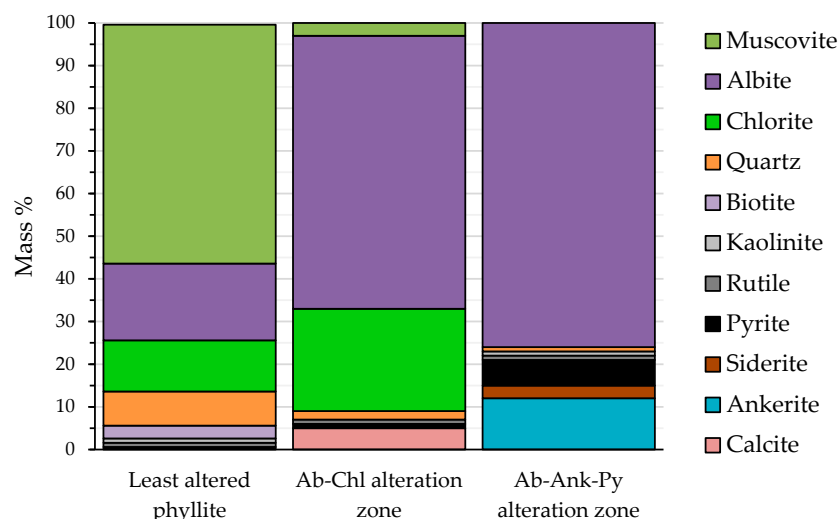


Figure 5. Mineral assembly in alteration zones. (Abbreviations: Ab = albite, Ank = ankerite, Chl = chlorite and Py = pyrite).

Table 1. Mineral quantification from different alteration zones measured by QEMSCAN.

Mineral (Mass %)	Least Altered Phyllite	Albite–Chlorite Alteration Zone	Albite–Ankerite–Pyrite Alteration Zone
Muscovite	56	3	0
Albite	18	64	76
Chlorite	12	24	0
Quartz	8	2	1
Biotite	3	0	0
Rutile	1	1	1
Kaolinite	1	0	1
Calcite	0	5	0
Ankerite	0	0	12
Siderite	0	0	3
Pyrite	1	1	6

In the distal albite–chlorite alteration zone, the model abundance of albite, chlorite and calcite reaches ~64, ~24 and ~5%, respectively. Relative to the least altered phyllite, muscovite is reduced by ~3 mass%, due to carbonatization and the replacement of muscovite by chlorite and albite. The abundance of quartz (~2%), rutile (~1%) and pyrite (~1%) is also reduced in this alteration zone. In the proximal albite–ankerite–pyrite alteration zone, albite (~76%) has almost totally replaced chlorite and muscovite as result of sodic metasomatism. Ankerite (~12%) is only formed in this alteration zone together with an increased amount of pyrite (~6%).

3.2. Bulk Geochemistry

The potassium contents of the samples from the least altered albite–chlorite alteration zone and albite–ankerite–pyrite alteration zone are represented by the decrease in K₂O of 3.37, 0.90 and 0.34 wt% (Table 2). This is inversely proportional to the sodium content (Na₂O), where the highest content is in albite–ankerite–pyrite alteration zone proximal to the veins, with a value of 7.93 wt%.

Table 2. Geochemical data of major oxides from different alteration zones measured by XRF.

No	Alteration Zone	SiO ₂	Fe ₂ O ₃	TiO ₂	Al ₂ O ₃	MnO	MgO	CaO	Na ₂ O	K ₂ O	P ₂ O ₅	SO ₃	Cr ₂ O ₃	LOI	Total
1	Least altered	56.56	6.83	0.90	18.91	0.17	2.06	0.51	0.89	3.37	0.14	bdl	bdl	8.48	99.00
2	Albite-chlorite	65.01	8.03	0.83	11.71	0.22	3.31	1.12	2.39	0.90	0.11	bdl	bdl	5.53	99.35
3	Albite-ankerite-pyrite	51.26	9.38	0.83	18.91	0.17	4.12	3.42	7.93	0.34	0.22	0.47	bdl	4.86	101.91

3.3. Mineral Chemistry

The mineral formulae were calculated from mineral chemistry measured by an electron microprobe analyzer (EPMA) using the characteristic analyses (Tables 3–5). Standard formulae were used for quartz, biotite and kaolinite due to the very small grain sizes [27,28].

Table 3. Mineral formulae calculated from electron microprobe analysis used for the balanced mineral reactions of least altered phyllite.

Element	Least Altered Phyllite							
	Albite	Quartz	Muscovite	Chlorite	Biotite	Pyrite	Rutile	Kaolinite
Si	2.950	1.000	3.306	2.926	2.803	0.000	0.015	1.978
Al	1.036	0.000	1.979	2.844	1.333	0.000	0.003	1.991
Ti	0.000	0.000	0.098	0.004	0.319	0.000	0.986	0.000
Fe	0.019	0.000	0.486	2.185	1.398	1.001	0.011	0.006
Mg	0.000	0.000	0.315	1.583	1.164	0.000	0.000	0.010
Ca	0.009	0.000	0.009	0.003	0.002	0.000	0.002	0.016
Na	0.937	0.000	0.433	0.006	0.021	0.000	0.000	0.021
K	0.007	0.000	0.365	0.043	0.989	0.000	0.000	0.023
Mn	0.001	0.000	0.014	0.078	0.007	0.000	0.000	0.000
O	8.000	2.000	11.000	18.000	12.000	0.000	2.000	9.000
C	0.000	0.000	0.000	0.000	0.000	0.000	0.000	0.000
S	0.000	0.000	0.000	0.000	0.000	1.999	0.000	0.000
H	0.000	0.000	2.000	8.000	2.000	0.000	0.000	4.000

3.4. Quantification of Mineral Reactions for Gains and Losses of Elements

Mineral–fluid reactions during alteration were identified by petrographic analysis. The dominant mineral reaction observed was the replacement of muscovite by albite. This replacement is caused by the reaction of the wall-rock with sodium- and silica-rich

hydrothermal fluids, as a result of which potassium and hydrogen cations and water are released according to following reaction:



Muscovite → Hydrothermal fluid → Albite

The gains and losses of elements during alteration was calculated from balanced mineral reactions for the various alteration zones [3]. Using the quantification of mineral data from the precursor rock and altered rock, the metasomatic process was evaluated by the components added to the system or lost from the system. The metasomatic reaction of muscovite replaced by albite was observed in the albite–ankerite–pyrite alteration zone (Figure 3c). By using the mineral formulae calculated from electron microprobe analysis (Table 5), and normalizing for Al, the reaction can be written as follows:

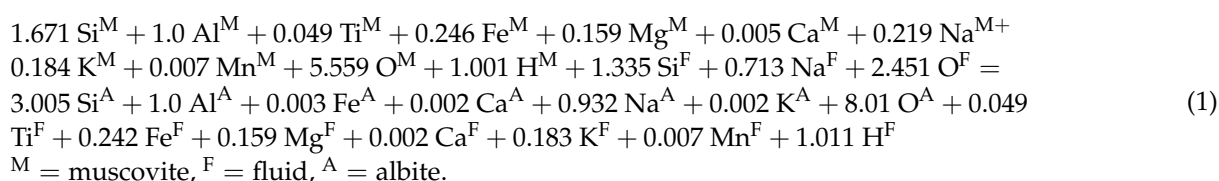


Table 4. Mineral formulae calculated from electron microprobe analysis used for the balanced mineral reactions of albite–chlorite alteration zone.

Element	Albite–Chlorite Alteration Zone						
	Albite	Quartz	Muscovite	Chlorite	Calcite	Pyrite	Rutile
Si	2.960	1.000	3.534	2.758	0.000	0.000	0.015
Al	1.071	0.000	1.989	2.553	0.000	0.000	0.003
Ti	0.000	0.000	0.001	0.001	0.000	0.000	0.986
Fe	0.015	0.000	0.201	2.304	0.002	1.001	0.011
Mg	0.000	0.000	0.299	2.304	0.001	0.000	0.000
Ca	0.017	0.000	0.004	0.009	0.993	0.000	0.002
Na	0.938	0.000	0.015	0.002	0.000	0.000	0.000
K	0.018	0.000	0.864	0.005	0.000	0.000	0.000
Mn	0.000	0.000	0.003	0.031	0.003	0.000	0.000
O	8.000	2.000	11.000	18.000	3.000	0.000	2.000
C	0.000	0.000	0.000	0.000	1.000	0.000	0.000
S	0.000	0.000	0.000	0.000	0.000	1.999	0.000
H	0.000	0.000	2.000	8.000	0.000	0.000	0.000

Table 5. Mineral formulae calculated from electron microprobe analysis used for the balanced mineral reactions of albite–ankerite–pyrite alteration zone.

Element	Albite–Ankerite–Pyrite Alteration Zone						
	Albite	Quartz	Muscovite	Chlorite	Ankerite	Siderite	Pyrite
Si	3.001	1.000	3.534	2.758	0.002	0.013	0.000
Al	0.999	0.000	1.989	2.553	0.000	0.000	0.000
Ti	0.000	0.000	0.001	0.001	0.000	0.000	0.000
Fe	0.003	0.000	0.201	2.304	0.413	0.626	1.001
Mg	0.000	0.000	0.299	2.304	0.537	0.296	0.000
Ca	0.002	0.000	0.004	0.009	0.991	0.025	0.000
Na	0.931	0.000	0.015	0.002	0.000	0.000	0.000
K	0.002	0.000	0.864	0.005	0.000	0.000	0.000
Mn	0.000	0.000	0.003	0.031	0.050	0.027	0.000
O	8.000	2.000	11.000	18.000	6.000	3.000	0.000
C	0.000	0.000	0.000	0.000	2.000	1.000	0.000
S	0.000	0.000	0.000	0.000	0.000	0.000	1.999
H	0.000	0.000	2.000	8.000	0.000	0.000	0.000

The metasomatic reaction in the albite–ankerite–pyrite alteration zone compared to the phyllite host rocks indicates that Fe, Ca, Mg, K, Mn, O and H were not completely removed by the fluid but were used to form other mineral phases such as ankerite, siderite and pyrite, involving more complex mineral–fluid reactions. The quantification of mineral reactions during hydrothermal alteration was calculated using the balanced mineral reac-

tion method [3,6,29] by combining the mass proportion (Table 1) and the mineral formulae calculated from electron microprobe analysis (Tables 3–5). These datasets were used to calculate the elemental composition of the rocks in mole/100 g.

Applying this method [3], the first step is to multiply the molar weight of the elements by their factor in the mineral formula. For example, SiO₂ has a Si factor of 1 and O factor of 2, used in order to calculate the elemental composition of the rocks in mole/100 g. The result is then multiplied by a factor determined from the modal abundance of the minerals in 100 g rock by dividing the molar weight with the modal abundance (in wt.%).

Gains and losses of elements defined from the difference in the elemental composition of the precursor rock and the altered rock were corrected for mass and volume changes. The calculation process involves iteration of a mass factor for the altered sample, minimizing the Al and Ti deficit and surplus, respectively, as immobile. The enrichment or depletion of elements by hydrothermal fluid during the alteration is interpreted by the difference between elemental compositions.

In the albite–chlorite alteration zone, the hydrothermal reaction involved a mass and volume increase of 14.5% and 0.6%, respectively, compared to the least altered phyllite. The balanced reaction indicates that the least altered phyllite reacted with the hydrothermal fluid, which added significant amounts of Si, Ca and Na to the system and removed K (Table 6 and Figure 6a). The alteration process involved 0.06 mole (0.69 g) CO₂, 0.01 mole (0.3 g) H₂S in the hydrothermal fluid and 0.1 mole (0.1 g) H₂O lost per 100 g from the least altered phyllite.

Table 6. Quantified compositional data for the least altered phyllite and the albite–chlorite alteration zone. The calculation was based on modal and mineral compositions balanced for immobile Al and a 14.5% mass increase. The difference indicates gain or loss/100 g for components and in % for volume changes in rock.

Element	Least Altered Phyllite								Total (g)		
	Ab	Qz	Ms	Chl	Bt	Py	Rt	Kn	100		
Si	0.20	0.13	0.48	0.06	0.02	0.00	0.00	0.01	0.89		
Al	0.07	0.00	0.28	0.05	0.01	0.00	0.00	0.01	0.43		
Ti	0.00	0.00	0.01	0.00	0.00	0.00	0.01	0.00	0.03		
Fe	0.00	0.00	0.07	0.04	0.01	0.00	0.00	0.00	0.13		
Mg	0.00	0.00	0.05	0.03	0.01	0.00	0.00	0.00	0.08		
Ca	0.00	0.00	0.00	0.00	0.00	0.00	0.00	0.00	0.00		
Na	0.06	0.00	0.06	0.00	0.00	0.00	0.00	0.00	0.13		
K	0.00	0.00	0.05	0.00	0.01	0.00	0.00	0.00	0.06		
Mn	0.00	0.00	0.00	0.00	0.00	0.00	0.00	0.00	0.00		
O	0.55	0.27	1.58	0.35	0.08	0.00	0.02	0.03	2.88		
C	0.00	0.00	0.00	0.00	0.00	0.00	0.00	0.00	0.00		
S	0.00	0.00	0.00	0.00	0.00	0.01	0.00	0.00	0.01		
H	0.00	0.00	0.29	0.15	0.01	0.00	0.00	0.02	0.47		
Mole	0.07	0.13	0.14	0.02	0.01	0.00	0.01	0.00			
molar vol.	100.45	22.69	140.57	210.57	152.10	23.95	18.69	99.35			
Vol. in rock	6.90	3.02	20.23	4.06	0.97	0.12	0.23	0.38	35.92		
Element	Albite–Chlorite Alteration Zone							Total (g)		Difference	
	Ab	Qz	Ms	Chl	Cal	Py	Rt	114.5		mole	Gram
Si	0.82	0.04	0.03	0.12	0.00	0.00	0.00	1.01	0.12	3.34	
Al	0.30	0.00	0.02	0.11	0.00	0.00	0.00	0.43	0.00	−0.01	
Ti	0.00	0.00	0.00	0.00	0.00	0.00	0.01	0.01	−0.01	−0.69	
Fe	0.00	0.00	0.00	0.10	0.00	0.01	0.00	0.12	−0.01	−0.62	
Mg	0.00	0.00	0.00	0.10	0.00	0.00	0.00	0.10	0.02	0.48	
Ca	0.00	0.00	0.00	0.00	0.06	0.00	0.00	0.06	0.06	2.40	
Na	0.26	0.00	0.00	0.00	0.00	0.00	0.00	0.26	0.13	3.07	
K	0.00	0.00	0.01	0.00	0.00	0.00	0.00	0.01	−0.05	−1.85	
Mn	0.00	0.00	0.00	0.00	0.00	0.00	0.00	0.00	0.00	−0.11	
O	2.22	0.08	0.10	0.79	0.17	0.00	0.03	3.38	0.50	8.01	
C	0.00	0.00	0.00	0.00	0.06	0.00	0.00	0.06	0.06	0.69	
S	0.00	0.00	0.00	0.00	0.00	0.02	0.00	0.02	0.01	0.30	
H	0.00	0.00	0.02	0.35	0.00	0.00	0.00	0.37	−0.10	−0.10	
Mole	0.24	0.03	0.01	0.04	0.05	0.01	0.01				
molar vol.	100.45	22.69	140.57	210.57	36.93	23.95	18.69				
Vol. in rock	24.37	0.76	1.10	8.03	1.84	0.20	0.23	36.53	0.61		

Abbreviation: Ab = albite, Bt = biotite, Cal = calcite, Chl = chlorite, Kn = kaolinite, Ms = muscovite, Py = pyrite, Qz = quartz, Rt = rutile.

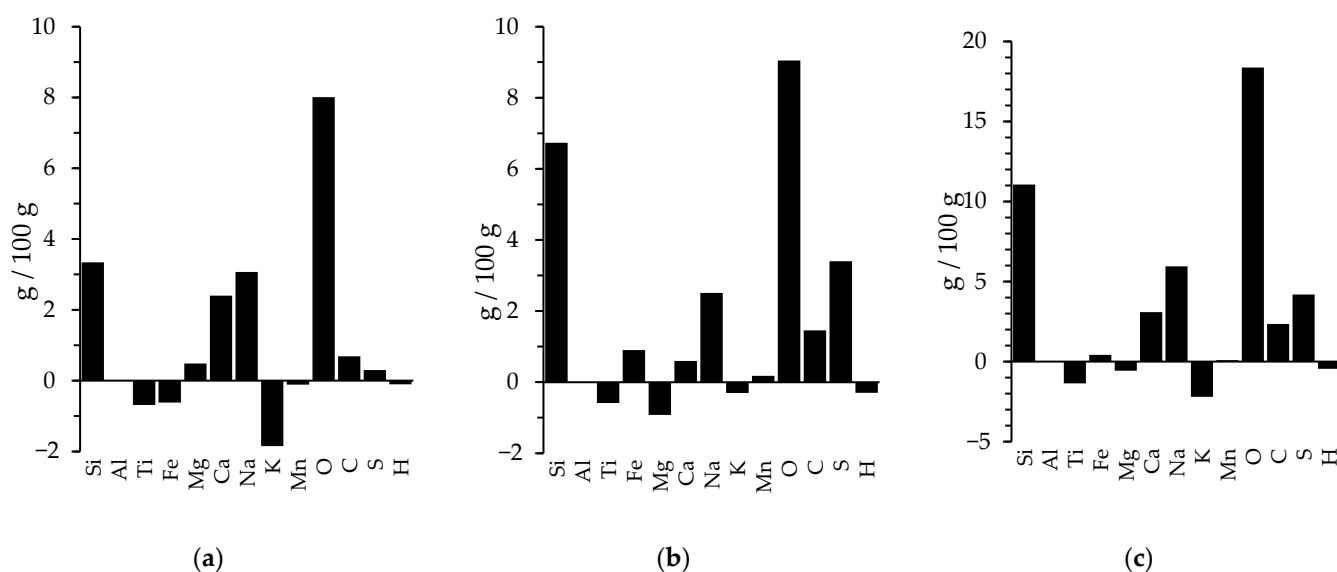


Figure 6. Gains and losses of elements during alteration of phyllites: (a) least altered phyllite to the albite–chlorite alteration zone, (b) albite–chlorite alteration zone to the albite–ankerite–pyrite alteration zone and (c) least altered phyllite to the albite–ankerite–pyrite alteration zone.

Alteration in the albite–ankerite–pyrite zone involved a mass increase of 22.7% and volume decrease of -0.1% compared to the albite–chlorite alteration zone. The reaction is represented by the significant addition of Si, Ca and Na, with the concomitant removal of Mg and K (Table 7 and Figure 6b). The balanced reaction indicates that 100 g precursor sample from the albite–chlorite alteration zone reacted with 0.12 mole (1.45 g) CO_2 and 0.11 mole (3.5 g) H_2S in the hydrothermal fluid and 0.3 mole (0.3 g) H_2O was released.

Table 7. Quantified compositional data for the albite–chlorite alteration zone and the albite–ankerite–pyrite alteration zone. The calculation was based on modal and mineral compositions balanced for immobile Al and a 22.7% mass increase. The difference indicates gain or loss/100 g for components and in % for volume changes in rock.

Element	Albite–Chlorite Alteration Zone							Total (g)
	Ab	Qz	Ms	Chl	Cal	Py	Rt	100
Si	0.72	0.03	0.03	0.11	0.00	0.00	0.00	0.88
Al	0.26	0.00	0.02	0.10	0.00	0.00	0.00	0.37
Ti	0.00	0.00	0.00	0.00	0.00	0.00	0.01	0.01
Fe	0.00	0.00	0.00	0.09	0.00	0.01	0.00	0.10
Mg	0.00	0.00	0.00	0.09	0.00	0.00	0.00	0.09
Ca	0.00	0.00	0.00	0.00	0.05	0.00	0.00	0.05
Na	0.23	0.00	0.00	0.00	0.00	0.00	0.00	0.23
K	0.00	0.00	0.01	0.00	0.00	0.00	0.00	0.01
Mn	0.00	0.00	0.00	0.00	0.00	0.00	0.00	0.00
O	1.94	0.07	0.09	0.69	0.15	0.00	0.02	2.95
C	0.00	0.00	0.00	0.00	0.05	0.00	0.00	0.05
S	0.00	0.00	0.00	0.00	0.00	0.02	0.00	0.02
H	0.00	0.00	0.02	0.31	0.00	0.00	0.00	0.32
Mole	0.24	0.03	0.01	0.04	0.05	0.01	0.01	
molar vol.	100.45	22.69	140.57	210.57	36.93	23.95	18.69	
Vol. in rock	24.37	0.76	1.10	8.03	1.84	0.20	0.23	36.53

Table 7. Cont.

Element	Albite–Ankerite–Pyrite Alteration Zone							Total (g)	Difference	
	Ab	Qz	Ms	Chl	Ank	Sd	Py	122.7	Mole	Gram
Si	1.09	0.02	0.01	0.01	0.00	0.00	0.00	1.12	0.24	6.73
Al	0.36	0.00	0.01	0.00	0.00	0.00	0.00	0.37	0.00	0.00
Ti	0.00	0.00	0.00	0.00	0.00	0.00	0.00	0.00	−0.01	−0.59
Fe	0.00	0.00	0.00	0.00	0.03	0.02	0.06	0.12	0.02	0.90
Mg	0.00	0.00	0.00	0.00	0.04	0.01	0.00	0.05	−0.04	−0.92
Ca	0.00	0.00	0.00	0.00	0.07	0.00	0.00	0.07	0.01	0.60
Na	0.34	0.00	0.00	0.00	0.00	0.00	0.00	0.34	0.11	2.51
K	0.00	0.00	0.00	0.00	0.00	0.00	0.00	0.00	−0.01	−0.31
Mn	0.00	0.00	0.00	0.00	0.00	0.00	0.00	0.00	0.00	0.17
O	2.90	0.04	0.04	0.04	0.41	0.11	0.00	3.52	0.57	9.05
C	0.00	0.00	0.00	0.00	0.14	0.04	0.00	0.17	0.12	1.45
S	0.00	0.00	0.00	0.00	0.00	0.00	0.12	0.12	0.11	3.40
H	0.00	0.00	0.01	0.02	0.00	0.00	0.00	0.02	−0.30	−0.30
Mole	0.30	0.02	0.00	0.00	0.06	0.03	0.05			
molar vol.	100.45	22.69	140.57	210.57	65.58	29.43	23.95			
Vol. in rock	29.64	0.38	0.37	0.33	3.63	0.84	1.20	36.38	−0.15	

Abbreviations: Ab = albite, Ank = ankerite, Bt = biotite, Cal = calcite, Chl = chlorite, Ms = muscovite, Py = pyrite, Qz = quartz, Rt = rutile and Sd—siderite.

The general metasomatic process during alteration from the least altered phyllite to the albite–ankerite–pyrite alteration zone involved a mass increase of 40.5% and volume increase of 0.47%. The reaction is represented by the significant addition of Si, Ca and Na, with the concomitant removal of Mg and K (Table 8 and Figure 6c).

Table 8. Quantified compositional data for the least altered phyllite and the albite–ankerite–pyrite alteration zone. The calculation was based on modal and mineral compositions balanced for immobile Al and a 40.5% mass increase. The difference indicates gain or loss /100 g for components and in % for volume changes in rock.

Element	Least Altered Phyllite								Total (g)
	Ab	Qz	Ms	Chl	Bt	Py	Rt	Kn	100
Si	0.20	0.13	0.48	0.06	0.02	0.00	0.00	0.01	0.89
Al	0.07	0.00	0.28	0.05	0.01	0.00	0.00	0.01	0.43
Ti	0.00	0.00	0.01	0.00	0.00	0.00	0.01	0.00	0.03
Fe	0.00	0.00	0.07	0.04	0.01	0.00	0.00	0.00	0.13
Mg	0.00	0.00	0.05	0.03	0.01	0.00	0.00	0.00	0.08
Ca	0.00	0.00	0.00	0.00	0.00	0.00	0.00	0.00	0.00
Na	0.06	0.00	0.06	0.00	0.00	0.00	0.00	0.00	0.13
K	0.00	0.00	0.05	0.00	0.01	0.00	0.00	0.00	0.06
Mn	0.00	0.00	0.00	0.00	0.00	0.00	0.00	0.00	0.00
O	0.55	0.27	1.58	0.35	0.08	0.00	0.02	0.03	2.88
C	0.00	0.00	0.00	0.00	0.00	0.00	0.00	0.00	0.00
S	0.00	0.00	0.00	0.00	0.00	0.01	0.00	0.00	0.01
H	0.00	0.00	0.29	0.15	0.01	0.00	0.00	0.02	0.47
Mole	0.07	0.13	0.14	0.02	0.01	0.00	0.01	0.00	
molar vol.	100.45	22.69	140.57	210.57	152.10	23.95	18.69	99.35	
Vol. in rock	6.90	3.02	20.23	4.06	0.97	0.12	0.23	0.38	35.92

Table 8. Cont.

Element	Albite–Ankerite–Pyrite alt. Zone							Total (g)	Difference	
	Ab	Qz	Ms	Chl	Ank	Sd	Py	140.5	Mole	Gram
Si	1.24	0.02	0.01	0.01	0.00	0.00	0.00	1.29	0.39	11.05
Al	0.41	0.00	0.01	0.01	0.00	0.00	0.00	0.43	0.00	0.00
Ti	0.00	0.00	0.00	0.00	0.00	0.00	0.00	0.00	−0.03	−1.36
Fe	0.00	0.00	0.00	0.01	0.03	0.03	0.07	0.13	0.01	0.41
Mg	0.00	0.00	0.00	0.01	0.04	0.01	0.00	0.06	−0.02	−0.57
Ca	0.00	0.00	0.00	0.00	0.08	0.00	0.00	0.08	0.08	3.09
Na	0.39	0.00	0.00	0.00	0.00	0.00	0.00	0.39	0.26	5.95
K	0.00	0.00	0.00	0.00	0.00	0.00	0.00	0.00	−0.06	−2.20
Mn	0.00	0.00	0.00	0.00	0.00	0.00	0.00	0.01	0.00	0.09
O	3.32	0.05	0.04	0.04	0.47	0.12	0.00	4.03	1.15	18.37
C	0.00	0.00	0.00	0.00	0.16	0.04	0.00	0.20	0.20	2.35
S	0.00	0.00	0.00	0.00	0.00	0.00	0.14	0.14	0.13	4.19
H	0.00	0.00	0.01	0.02	0.00	0.00	0.00	0.03	−0.45	−0.45
Mole	0.30	0.02	0.00	0.00	0.06	0.03	0.05			
molar vol.	100.45	22.69	140.57	210.57	65.58	29.43	23.95			
Vol. in rock	29.64	0.38	0.37	0.33	3.63	0.84	1.20	36.38	0.47	

Abbreviation: Ab = albite, Ank = ankerite, Bt = biotite, Cal = calcite, Chl = chlorite, Kn = kaolinite, Ms = muscovite, Py = pyrite, Qz = quartz, Rt = rutile, Sd = siderite.

4. Discussion

Petrographic analyses of the least altered phyllite and the associated alteration zones testify to hydrothermal mineral alteration reactions. The dominant modal change from the least altered phyllite to the albite–chlorite alteration zone is the replacement of muscovite by albite, indicating infiltration of sodium-rich hydrothermal fluids. Next to albite, Mg chlorite was also a stable component. Elemental gains include Si, Na, Ca, minor Mg, carbonate and minor S, while Ti, Fe and K were depleted.

Comparison of chemical changes in the alteration zones generally indicate addition of O, Si, Ca and particularly Na. Closer to the mineralized zone, the sodium content increases while potassium decreases. The metasomatic reaction leading from the albite–chlorite alteration zone to the albite–ankerite–pyrite alteration zone shows significant addition of Si, Ca, Na, Fe, carbonate and S with the concomitant removal of Mg and K. This results in the formation of albite, ankerite and pyrite mineral assemblage.

Elemental changes between the least altered phyllite and the albite–ankerite–pyrite alteration zone display a similar pattern. There is a significant addition of Si, Ca, Na, carbonate, minor Fe and S, with the related removal of Mg and K. Mineralogically, muscovite was almost totally replaced by albite, with only some rare relics of muscovite sporadically observed in thin sections. Pyrite formed by the reaction of Fe with H₂S. Although minor amounts of Fe were introduced by the external fluids, the decomposition of chlorite provided sufficient Fe for pyrite formation [22,23].

The textural preservation and very low volume changes during alteration of wall-rocks may indicate isovolumetric reactions during metasomatism [30,31]. Albitization is the dominant alteration both in the proximal and distal alteration zone followed by variable degrees of carbonatization (ankerite and siderite) and sulfidation (pyrite, minor galena and chalcopyrite).

The orogenic Au literature describes the typical mineralization-associated metasomatic enrichment of potassium and the hydrolysis of feldspar to form mica minerals [32–35]. In contrast, sodic alteration is not very commonly associated with orogenic gold deposits, but has been noted elsewhere [36,37]. The origin of Na and/or Ca enrichment in some orogenic fluids is still disputed, and interaction of fluids with altered ultramafic rocks in the basement sequence has been suggested [29,38,39]. For Awak Mas, we rather propose the origin of the sodium-rich fluids is from metamorphic dewatering of marine sedimentary sequences and, as the deposits was formed at shallow depths, from related basinal brines [22].

At Awak Mas, albite veining overprints muscovite in the least altered phyllite to form the distal and proximal alteration zones. This may have initiated a failure mode transition from ductile to brittle failure, with consequences for the focusing of fluid flow [22].

If we assume gold transport by the bisulfide complex, as is generally suggested for orogenic gold deposits, the formation of pyrite in the alteration zone could have enabled gold precipitation, since the depletion of sulfur in the fluids may have caused the destabilization of the dissolved Au–S complex [40–45]. The presence of ankerite as a result of reaction between CO₂-bearing hydrothermal fluids with chlorite in the proximal alteration zone is one of the characteristics of orogenic gold deposits [46,47].

5. Conclusions

Mass balance calculations are useful tools for quantifying element changes during metasomatic processes, relative to the unaltered or least-altered rock, representing the protolith. At Awak Mas, the predominant petrographic manifestation of this process is the replacement of muscovite by albite. Calculated elemental gains and losses allowed conclusions on the chemical make-up of the hydrothermal fluids to be made, which were enriched in Si, Ca, Na, CO₂, minor Fe and S, but depleted in Mg and K. This information helped to suggest that the mineralizing fluids originated from metamorphic dewatering of marine sedimentary sequences, and probably from related basinal brines. The very low volume changes indicated by the mass balance calculations are supported by the observed textural preservation, pointing to isovolumetric metasomatic reactions.

In general, this study improves the geochemical understanding of element mobility in epizonal orogenic Au deposits by presenting mass balance calculations that address the compositional heterogeneity of protolith and altered rocks.

Author Contributions: Conceptualization, E.E., A.I. and F.M.M.; methodology, E.E., A.I. and F.M.M.; software, E.E.; validation, E.E., A.I. and F.M.M.; formal analysis, E.E.; investigation, E.E.; writing—original draft preparation, E.E. and A.I.; writing—review and editing, E.E., A.I. and F.M.M.; visualization, E.E. All authors have read and agreed to the published version of the manuscript.

Funding: This research was funded by The Ministry of Energy and Mineral Resources, Republic of Indonesia, letter of assignment number 2917K/69/MEM/2013.

Data Availability Statement: Data available on request due to company confidentiality.

Acknowledgments: The authors thank the management of Masmino Dwi Area Company for their permission to use their data and samples for this study. For most of the analytical work, the facilities of the Institute of Applied Mineralogy and Economic Geology, RWTH Aachen University were used. Help with QEMSCAN and EPMA measurements from Lars Gronen and Roman Klinghardt is gratefully acknowledged.

Conflicts of Interest: The authors declare no conflict of interest.

References

1. Gresens, R.L. Composition-volume relationships of metasomatism. *Chem. Geol.* **1967**, *2*, 47–65. [[CrossRef](#)]
2. Grant, J.A. The isocon diagram; a simple solution to Gresens' equation for metasomatic alteration. *Econ. Geol.* **1986**, *81*, 1976–1982. [[CrossRef](#)]
3. Kolb, J.; Meyer, F.M. Balanced mineral reactions for alteration zones developed in auriferous shear zones of the Hutti Mine, Dharwar Craton, India. *Z. Dtsch. Ges. Geowiss.* **2008**, *159*, 331–347. [[CrossRef](#)]
4. Kerrich, R.; Fyfe, W.S.; German, B.E.; Allison, I. Local modification of rock chemistry by deformation. *Contrib. Miner. Petrol.* **1977**, *65*, 183–190. [[CrossRef](#)]
5. Baumgartner, L.P.; Olsen, S.N. A least-squares approach to mass transport calculations using the isocon method. *Econ. Geol.* **1995**, *90*, 1261–1270. [[CrossRef](#)]
6. Mountain, B.W.; Williams-Jones, A.W. Mass transfer and the path of metasomatic reactions in mesothermal gold deposits; an example from Flambeau Lake, Ontario. *Econ. Geol.* **1996**, *91*, 302–321. [[CrossRef](#)]
7. Kretz, R. Redistribution of major and trace elements during the formation of biotite–plagioclase reaction zones at boundaries between amphibolite and K-feldspar gneiss, Otter Lake area, Quebec, Canada. *Canad. Miner.* **2000**, *38*, 525–543. [[CrossRef](#)]

8. Idrus, A.; Kolb, J.; Meyer, F.M. Mineralogy, lithogeochemistry and elemental mass balance of the hydrothermal alteration associated with the gold-rich Batu Hijau porphyry copper deposit, Sumbawa Island, Indonesia. *Resour. Geol.* **2009**, *59*, 215–230. [[CrossRef](#)]
9. Dipple, G.M.; Ferry, J.M. Metasomatism and fluid flow in ductile fault zones. *Contrib. Miner. Petrol.* **1992**, *112*, 149–164. [[CrossRef](#)]
10. Taylor, H.P., Jr. Oxygen and hydrogen isotope relationships in hydrothermal mineral deposits. *Geochem. Hydr. Ore Dep.* **1979**, *1979*, 236–277.
11. de Groot, P.A. *Water/Rock Ratio Calculations in Hydrothermal Systems: A Case Study from Bergslagen, Central Sweden*; No. 314; Economic Geology Research Unit, Department of Geology, University of the Witwatersrand: Johannesburg, South Africa, 1997.
12. Parkinson, C.D. An outline of the petrology, structure and age of the Pompangano Schist Complex of central Sulawesi, Indonesia. *Isl. Arc* **1998**, *7*, 231–245. [[CrossRef](#)]
13. Elburg, M.; van Leeuwen, T.M.; Foden, J. Spatial and temporal isotopic domains of contrasting igneous suites in western and northern Sulawesi, Indonesia. *Chem. Geol.* **2003**, *199*, 243–276. [[CrossRef](#)]
14. van Leeuwen, T.M.; Allen, C.M.; Kadarusman, A.; Elburg, M.; Palin, J.M. Petrologic, isotopic, and radiometric age constraints on the origin and tectonic history of the Malino Metamorphic Complex, NW Sulawesi, Indonesia. *J. Asian Earth Sci.* **2007**, *29*, 751–777. [[CrossRef](#)]
15. Cottam, M.A.; Hall, R.; Forster, M.A.; Boudagher-Fadel, M.K. Basement character and basin formation in Gorontalo Bay, Sulawesi, Indonesia: New observations from the Togian Islands. *J. Geol. Soc. Lond.* **2011**, *355*, 177–202. [[CrossRef](#)]
16. White, L.T.; Hall, R.; Armstrong, R.A.; Barber, A.J.; Fadel, M.B.; Baxter, A.; Wakita, K.; Manning, C.; Soesilo, J. The geological history of the Latimojong region of western Sulawesi, Indonesia. *J. Asian Earth Sci.* **2017**, *138*, 72–91. [[CrossRef](#)]
17. Archibald, N.J.; Power, W.L.; Ketelaar, P.B.; Utley, D.C.; Panizza, N.; Nichols, S.N. Geology of the Awak Mas prospect area, south central Sulawesi, Indonesia. Unpublished Internal Report of PT Masmindo Eka Sakti, Jakarta. 1996.
18. Querubin, C.D.; Waters, S. Geology and mineralization of Awak Mas: A sedimentary hosted gold deposit, South Sulawesi, Indonesia. *Maj. Geol. Ind.* **2012**, *27*, 69–85.
19. Djuri, S.; Bachri, S. *Geological Map of the Majene and The Western Part of Palopo Sheets, Sulawesi, Scale 1, 250,000*; Geological Research and Development Centre: Bandung, Indonesia, 1998.
20. Tuakia, M.Z.; Takahashi, R.; Imai, A. Geological and Geochemical Characteristics of Gold Mineralization in the Salu Bulu Prospect, Sulawesi, Indonesia. *Resour. Geol.* **2019**, *69*, 176–192. [[CrossRef](#)]
21. Al Hakim, A.Y.; Melcher, F.; Prochaska, W.; Bakker, R.; Rantitsch, G. Formation of epizonal gold mineralization within the Latimojong Metamorphic Complex, Sulawesi, Indonesia: Evidence from mineralogy, Fluid inclusions and Raman spectroscopy. *Ore Geol. Rev.* **2018**, *97*, 88–108. [[CrossRef](#)]
22. Ernowo, E.; Meyer, F.M.; Idrus, A. Hydrothermal alteration and gold mineralization of the Awak Mas metasedimentary rock-hosted gold deposit, Sulawesi, Indonesia. *Ore Geol. Rev.* **2019**, *113*, 103083. [[CrossRef](#)]
23. Ernowo. Hydrothermal Alteration and Gold Mineralization of the Awak Mas Gold Deposit, Sulawesi Island, Indonesia. Dissertation's Thesis, RWTH Aachen University, Aachen, Germany, 2017.
24. Gottlieb, P.; Wilkie, G.; Sutherland, D.; Ho-Tun, E.; Suthers, S.; Perera, K.; Rayner, J. Using quantitative electron microscopy for process mineralogy applications. *Jom* **2000**, *52*, 24–25. [[CrossRef](#)]
25. Pirrie, D.; Butcher, A.R.; Power, M.R.; Gottlieb, P.; Miller, G.L. Rapid quantitative mineral and phase analysis using automated scanning electron microscopy (QemSCAN); potential applications in forensic geoscience. *J. Geol. Soc. Lond.* **2004**, *232*, 123–136. [[CrossRef](#)]
26. Sindern, S.; Meyer, F.M. Automated quantitative rare earth elements mineralogy by scanning electron microscopy. In *Handbook of Rare Earth Elements: Analytics*; Walter de Gruyter GmbH & Co KG: Berlin, Germany, 2017.
27. Bohlen, S.R.; Eric, J.E. Evaluation of coexisting garnet-biotite, garnet-clinopyroxene, and other Mg-Fe exchange thermometers in Adirondack granulites. *Geol. Soc. Am. Bull.* **1980**, *91*, 685–719. [[CrossRef](#)]
28. Kerr, P.F. *Analytical Data on Reference Clay Materials. No. 7*; Columbia University: New York, NY, USA, 1950.
29. Böhlke, J.K. Comparison of Metasomatic Reactions Between a Common CO₂-Rich Vein Fluid and Diverse Wall Rocks. Intensive Variables, Mass Transfers, and Au Mineralization at Alleghany. *Cal. Econ. Geol.* **1989**, *84*, 291–327. [[CrossRef](#)]
30. Selverstone, J.; Morteani, G.; Staude, J.M. Fluid channeling during ductile shearing: Transformation of granodiorite into aluminous schist in the Tauern Window, Eastern Alps. *J. Metamorph. Geol.* **1991**, *9*, 419–431. [[CrossRef](#)]
31. McCaigh, A.M. The geochemistry of volatile fluid flow in shear zones. Deformation enhanced fluid transport in earth's crust and mantle. *M.B. Holmes Miner. Sic. Ser. Lond.* **1997**, *8*, 227–266.
32. Wang, R.; Cudahy, T.; Laukamp, C.; Walshe, J.L.; Bath, A.; Mei, Y.; Young, C.; Roache, T.J.; Jenkins, A.; Roberts, M.; et al. White mica as a hyperspectral tool in exploration for the Sunrise Dam and Kanowna Belle gold deposits, Western Australia. *Econ. Geol.* **2017**, *112*, 1153–1176.
33. Bogossian, J.; Hagemann, S.G.; Rodrigues, V.G.; Lobato, L.M.; Roberts, M. Hydrothermal alteration and mineralization in the Faina greenstone belt: Evidence from the Cascavel and Sertão orogenic gold deposits. *Ore Geol. Rev.* **2020**, *119*, 103293. [[CrossRef](#)]
34. Zoheir, B.; Feigenson, M.; Zi, J.W.; Turrin, B.; Deshesh, F.; El-Metwally, A. Ediacaran (~600 Ma) orogenic gold in Egypt: Age of the Atalla gold mineralization and its geological significance. *Int. Geol. Rev.* **2019**, *61*, 779–794. [[CrossRef](#)]
35. Wilde, A.R.; Bierlein, F.P.; Pawlitschek, M. Lithogeochemistry of orogenic gold deposits in Victoria, SE Australia: A preliminary assessment for undercover exploration. *J. Geochem. Explor.* **2004**, *84*, 35–50. [[CrossRef](#)]

36. Morasse, S.; Hodgson, C.J.; Guha, J.; Coulombe, A. Oxidative, alkali-amphibole-bearing alteration and its relation to gold in the senite-associated Lac Shortt deposit, Abitibi greenstone belt, Quebec, Canada. In *Bicentennial Gold 88: Extended Abstracts*; Geological Society of Australia: Sydney, Australia, 1988; Volume 1, pp. 92–94.
37. Albino, G.V. Sodium metasomatism along the Melones Fault Zone, Sierra Nevada Foothills, California, USA. *Miner. Mag.* **1995**, *59*, 383–399. [[CrossRef](#)]
38. Coveney, R.M., Jr. Gold quartz veins and auriferous granite at the Oriental mine, Alleghany district, California. *Econ. Geol.* **1981**, *76*, 2176–2199. [[CrossRef](#)]
39. Böhlke, J.K.; Kistler, R.W. Rb-Sr, K-Ar, and stable isotope evidence for the ages and sources of fluid components of gold-bearing quartz veins in the northern Sierra Nevada foothills metamorphic belt, California. *Econ. Geol.* **1986**, *81*, 296–322. [[CrossRef](#)]
40. Phillips, G.N.; Groves, D.J. The nature of Archaean gold bearing fluids as deduced from gold deposits of Western Australia. *J. Geol. Soc. Aust.* **1993**, *30*, 25–39. [[CrossRef](#)]
41. Groves, D.L.; Phillips, G.N.; Ho, S.E.; Houstoun, S.M. The nature, genesis and regional controls of gold mineralization in Archaean greenstone belts of the Western Australian Shield; a brief review. *S. Afr. J. Geol.* **1985**, *88*, 135–148.
42. Mikucki, E.J. Hydrothermal transport and depositional processes in Archean lode-gold systems: A review. *Ore Geol. Rev.* **1998**, *13*, 307–321. [[CrossRef](#)]
43. Stefansson, A.; Seward, T.M. Stability of chloride gold(I) complexes in aqueous solutions from 300 to 600 °C and from 500 to 1800 bar. *Geochim. Cosmochim. Acta* **2003**, *67*, 4559–4576. [[CrossRef](#)]
44. Stefansson, A.; Seward, T.M. Gold(I) complexing in aqueous sulphide solutions to 500 °C at 500 bar. *Geochim. Cosmochim. Acta* **2004**, *68*, 4121–4143. [[CrossRef](#)]
45. Phillips, G.N.; Powell, R. Formation of gold deposits: A metamorphic devolatilization model. *J. Metamorph. Geol.* **2010**, *28*, 689–718. [[CrossRef](#)]
46. McCuaig, T.C.; Kerrich, R. P–T–Deformation—Fluid characteristics of lode gold deposits: Evidence from alteration systematics. *Ore Geol. Rev.* **1998**, *12*, 381–453. [[CrossRef](#)]
47. Craw, D.; Upton, P.; MacKenzie, D.J. Hydrothermal alteration styles in ancient and modern orogenic gold deposits, New Zealand. *N. Z. J. Geol. Geophys.* **2009**, *52*, 11–26. [[CrossRef](#)]